Article

J. Biol. Regul. Homeost. Agents. 2024; 38(5): 4335–4348
https://doi.org/10.23812/j.biol.regul.homeost.agents.20243805.344

Polygala Fallax Hemsl Ameliorates Renal Dysfunction and Podocyte Mitochondrial Oxidative Damage in Diabetic Rats by Activating the AMPK/SIRT1/PGC-1α Signaling

Shih-wei Chao[1,*], Yanhua Yi[2,3], Weiling Chen[4], Huiping Tang[5], Bo Chen[6]

[1]Department of Traditional Chinese Medicine, Guilin Hospital of the Second Xiangya Hospital Central South University, 541003 Guilin, Guangxi, China
[2]Department of Burn, Would Repair Surgery and Plastic Surgery, Affiliated Hospital of Guilin Medical University, 541001 Guilin, Guangxi, China
[3]Department of Aesthetic Surgery, Affiliated Hospital of Guilin Medical University, 541001 Guilin, Guangxi, China
[4]Department of Gynecology, Sinopharm Tongmei General Hospital, 037001 Datong, Shanxi, China
[5]Department of Traditional Chinese Medicine, Guilin Hospital of the Second Xiangya Hospital CSU, 541006 Guilin, Guangxi, China
[6]School of Clinical Medicine, Guilin Medical University, 541001 Guilin, Guangxi, China
*Correspondence: 17777349004@163.com (Shih-wei Chao)
Published: 1 May 2024

Backgrounds: Diabetic nephropathy (DN) is a microvascular disease affecting the glomeruli and renal tubules, resulting from diabetes mellitus. Our present experiment was designed to assess the potential therapeutic of Polygala fallax Hemsl (PFH) on DN in diabetic rats.

Methods: As a model of DN, Sprague-Dawley (SD) rats were fed a high-sugar, high-fat diet with streptozotocin (STZ) intraperitoneally injected. The rats that exhibited successful modeling were randomly allocated into different groups, including the model group, as well as PFH low (2 g/kg), medium (4 g/kg), and high (8 g/kg) dose groups. Additionally, there was a positive drug group treated with Losartan Possaium (LP) at a dosage of 16 mg/kg. The general condition of rats was observed, and biochemical tests were conducted. Histopathological changes in renal tissue were assessed using staining techniques such as Hematoxylin-eosin (H&E), periodic acid-Schiff (PAS), and Masson staining. Immunofluorescence (IF), immunohistochemistry (IHC), and Western blot analyses were utilized to assess protein expression levels in renal tissue.

Results: Intragastric administration of PFH for 4 weeks in diabetic rats dose-dependently decreased renal weight/body weight ($p < 0.05$ or $p < 0.01$), insulin resistance ($p < 0.05$ or $p < 0.01$), total cholesterol (TC; $p > 0.05$ or $p < 0.01$), triglyceride (TG; $p < 0.05$ or $p < 0.01$), serum albumin (ALB; $p < 0.01$), creatinine (CREA; $p < 0.05$ or $p < 0.01$), carbamide (UREA; $p < 0.01$), alanine aminotransferase (ALT; $p < 0.01$), aspartate aminotransferase (AST; $p < 0.05$ or $p < 0.01$) levels. PFH significantly inhibited podocyte damage, basement membrane thickening, renal tubular epithelial cell swelling, and inflammatory cell infiltration. Moreover, PFH dose-dependently promoted mitochondrial membrane potential (MMP; $p < 0.05$ or $p < 0.01$) and inhibited reactive oxygen species (ROS; $p < 0.01$) generation, podocyte apoptosis ($p < 0.01$), mitochondrial fragmentation, and dysfunction *in vivo*. Besides, the high-dose PFH treatment group had a similar improvement effect on podocyte mitochondrial damage andapoptosis as the positive drug control group. Mechanistically, PFH could stabilize mitochondrial morphology in podocytes via activation of AMP-activated protein kinase (AMPK)/silent information regulator sirtuin 1 (SIRT1)/peroxisome proliferator-activated receptor-gamma coactivator (PGC)-1α signaling.

Conclusion: Thus, PFH mitigated mitochondrial dysfunction and oxidative damage in renal podocytes of DN rats, thereby safeguarding renal function. This protective mechanism is believed to involve the mobilisation of the AMPK/SIRT1/PGC-1α axis.

Keywords: Polygala fallax Hemsl; AMPK/SIRT1/PGC-1α signaling; podocyte damage; Diabetic nephropathy

Introduction

Diabetic nephropathy (DN), a prominent complication of diabetes, has been recognized as the leading cause for the progression of chronic kidney disease and end-stage renal failure [1]. Approximately 30–50% of individuals diagnosed with diabetes worldwide eventually have develop end-stage renal disease (ESRD) [2]. DN can be caused by hyperglycemia, abnormal metabolism of blood lipids, microvascular circulation disorders, and inflammatory reactions [3]. The primary pathological characteristics of DN encompass glomerular hypertrophy, podocyte loss, glomerular sclerosis, and fusion of foot processes [4]. The main clinical manifestations are chronic hyperglycemia and proteinuria [5]. Podocyte injury is a crucial factor in the pathogenesis and advancement of DN [6]. Podocytes are

Journal of
BIOLOGICAL REGULATORS
and Homeostatic Agents

highly specialized terminally differentiated cells whose reduced numbers and abnormal functional morphology contribute significantly to the pathogenesis of DN [7,8]. Thus, reducing podocyte damage represents a critical therapeutic strategy for alleviating DN.

Accumulating data show that traditional Chinese medicine is beneficial for treaing DN because of its various effects and overall regulatory effects [9,10]. Polygala fallax Hemsl (PFH) is a perennial Leaf bush belonging to the Polygalaceae family. The main chemical components of PFH include flavonoids and saponins, which have significant pharmacological effects such as lowering blood lipids, anti-oxidation, improving ovarian endometriosis, and anti-inflammatory and antiviral effects [11–14]. A previous study demonstrated that combination therapy of compound Sanqi granules and PFH exerted a therapeutic effect on glomerulonephritis by suppressing mesangial cell proliferation while inducing apoptosis in human mesangial cells [12]. Moreover, PFH exhibited significant protective effects against high glucose (HG)-induced human glomerular mesangial cell (HMC) proliferation, apoptosis, and inflammation by effectively inhibiting activation of the toll-like receptor 4-dependent nuclear factor-kappa B signaling pathway [15]. However, *in vivo* effects of PFH on DN have not been reported.

Herein, we examined the effectiveness and mechanism of PFH-mediated renal protection in a rat model of DN induced by streptozotocin (STZ) and a high-fat diet. The findings demonstrat that PFH played a beneficial role in the recovery of DN by mediating renal podocyte inflammation and autophagy.

Methods and Materials

Ultra-Performance Liquid Chromatography-Mass Spectrometry (UPLC-MS) Analysis

PFH was purchased from Jiaheng Lengbei Yaoye (Ji201730004, Baoding, China). The chemical composition of PFH was analyzed using UPLC-MS coupled with a hybrid Quadrupole-TOF LC/MS/MS Mass Spectrometer (B Sciex Instruments, Shimadzu LC30, Applied Biosystems, Inc., Columbia, MA, USA) equipped with a ChromCore 120 C18 Column (1.8 µm, 150 × 2.1 mm) maintained at a column temperature of 40 °C. A gradient elution method was utilized with the mobile phase consisting of 0.1% formic acid (A) and 100% acetonitrile (B), flowing at a rate of 0.3 mL/min as follows: 0 min, 5% B; 10 min, 70% B; 17 min, 100% B; 18 min, 100% B; 19 min, 5% B; 21 min, 5% B. Mass spectra in the WIFF format were analyzed using MS-DIAL 4.70 (RIKEN, Yokohama, Japan). Spectra for the most prominent peaks were compared to database entries in MassBank, ReSpect, and GNPS for identification.

Animals

Thirty-six specific-pathogen-free male Sprague-Dawley (SD) rats, aged 6–8 weeks and weighing 200–250 g, were procured from Dashuo Animal Experiment Co., Ltd. (Chengdu, Sichuan). The rats were kept in a controlled environment with minimal temperature fluctuations, maintaining an average temperature of approximately 25 °C. The relative humidity levels ranged between 50% and 60%, and the rats were exposed to a consistent light/dark cycle lasting for 12 h each. Additionally, rats received food and water ad libitum. All procedures were conducted in compliance with the updated Animals (Scientific Procedures) Act of 1986 within the United Kingdom, as well as Directive 2010/63/EU across Europe. The study protocols were approved by the Ethics Committee of Guilin Hospital of the Second Xiangya Hospital Central South University (No. 20210710).

Model Establishment and Therapy

Rats were fasted overnight (from 8:00 PM to 8:00 AM) before STZ modeling. Six rats were assigned to the control group, where they were given a regular diet. The other groups received a high-fat diet for 6 weeks, after which they were intraperitoneally injected with 55 mg/kg STZ for modeling. The control group received an intraperitoneal injection of citrate buffer at an equivalent dosage. After STZ injection, 15 g/L sucrose water was given for 48 h to reduce the death rate. After 72 h of STZ injection, fasting blood glucose (FBG) levels were 250 mg/dL, indicating successful induction of diabetes in the model [16]. The model rats were subcutaneously injected with long-acting insulin (insulin glargine injection, J20140052, SANOFI, Beijing, China) (2–4 U/rat) to maintain blood glucose between 16–33 mmol/L and avoid ketosis. After establishing the DN model, rats were randomly allocated into five groups (n = 6 rats/group): Diabetic nephropath (DN) model group, low-dose PFH group (PFH-low), medium-dose PFH group (PFH-medium), high-dose PFH group (PFH-high), and positive drug Losartan Potassium (LP) group. The control group and DN model group were orally administered saline. Meanwhile, low, medium, and high PFH groups received 2, 4, and 8 g/kg of PFH, respectively. Rats in the LP group were given 16 mg/kg of LP. The rats were treated once a day for 4 weeks.

Specimen Collection

After 4 weeks of drug intervention, blood samples were collected from the tail vein of fasting rats to measure FBG. Rats were anesthetized by intraperitoneal injection of 3% pentobarbital sodium at a dosage of 40 mg/kg. Femoral arterial blood was then collected for the detection of renal function indexes. Rats were euthanized by 100% CO_2 asphyxiation and cervical dislocation. Anesthesia and euthanasia procedures complied with the American Veterinary Medical Association guidelines (2013). Both kidneys

were removed and rinsed with normal saline. An incision was made along the longitudinal axis. About 5 mm of the right kidney cortex was placed in 4% paraformaldehyde and fixed for Hematoxylin-eosin (H&E), Masson's trichrome, and periodic acid-Schiff (PAS) staining, and immunohistochemistry (IHC) detection. Approximately 1 mm^3 pieces of the left renal cortex were placed in 2.5% glutaraldehyde and frozen in a 4 °C refrigerator for transmission electron microscopy sample preparation. About 3 mm^3 pieces of the left kidney cortex were placed in a frozen tube, rapidly frozen using liquid nitrogen, and stored in a –80 °C refrigerator.

H&E Staining

Renal tissues were preserved in 4% paraformaldehyde overnight. Subsequently, samples were processed and embedded in paraffin. The tissue sections (5 μm) were dewaxed twice with toluene, dehydrated with ethanol, washed with distilled water, and then stained with hematoxylin. After rinsing, slices were separated using an alcohol solution containing 1% hydrochloric acid, stained with eosin, and then with distilled water for 10 min. Slices were dehydrated using xylene and then sealed using a neutral glue. The results were examined using a digital trinocular camera microscope at 100× and 400× magnifications (BA210Digital, Motic, Beijing, China).

Masson's Trichrome Staining

The kidney paraffin sections were stained with hematoxylin for 5 min. Subsequently, sections were restored to a blue color using 0.6% ammonia water. Sections were further differentiated with a 1% phosphomolybdate aqueous solution, followed by a 5-min exposure to aniline blue dye. Finally, differentiation was accomplished using a 1% acetic acid aqueous solution. After rinsing with running water, slices were dehydrated, made transparent, and sealed, and image acquisition was performed using a microscope (BA210Digital, Motic, Beijing, China). The fibrous tissue area (Area) in the acquired images was measured using the Image-pro Plus 6.0 Image analysis system (Media Cybernetics, Inc., Rockville, MD, USA), and the fibrous tissue expression area was calculated as the ratio of fibrous tissue area to the visual field area.

PAS Staining

Part of the prepared paraffin sample was sliced and dewaxed to water by routine. Subsequently, it was treated with a permanganate alcohol solution for 10 min and then rinsed with 70% ethanol. The sample was then exposed to a reducing solution for 1 min and then rinsed with 70% ethanol. Finally, the sample was treated with a colorless basic fuchsin solution for 1 h. The positive expression area (Area) in the acquired images was quantified utilizing the Image-pro Plus 6.0 Image analysis system (Media Cybernetics, Inc., Rockville, MD, USA). Subsequently, the positive expression area was determined by dividing it by the visual field area.

Transmission Electron Microscopy (TEM)

TEM was utilized to observe podocyte mitochondrial injury. Renal tissue samples were initially fixed with a 3% glutaraldehyde solution and subsequently postfixed in a 1% osmium tetroxide solution for 2 h. Next, a gradient acetone technique was employed to remove moisture from the samples before they were embedded in Epon812 (M039005, Micxy Reagent, Chengdu, China). Using an ultramicrotome, ultrathin sections with a thickness of 1 mm were cut and stained with toluidine blue. Ultrathin sections measuring 70 nm in thickness were obtained using a diamond knife. After staining with uranium acetate and lead citron citrate, samples were analyzed using a TEM apparatus (JEM-1400Flash, JEOL, Akishima, Japan).

IHC Staining

Renal tissue sections were routinely dewaxed and hydrated with gradient ethanol before treatment with antigen repair solution at 95–99 °C for 40 min. After washing thrice, a cleaved-caspase-3 antibody (1:400, Cat. A22672, Abclonal, Wuhan, China) or a caspase-3 antibody (1:200, Cat. GB11009-1-100, Servicebio, Wuhan, China) was added and incubated at 4 °C overnight. On the next day, samples were incubated with a corresponding secondary antibody (1:100, Cat. B23303, Servicebio, Wuhan, China) for 1 h. Then the Envision detection and color development kit was used for 3,3′-diaminobenzidine (DAB) color development. IHC images were evaluated microscopically (BA400Digital, Motic Instruments, Inc., Baltimore, MD, USA).

Immunofluorescence (IF) Staining

Renal tissue sections were dewaxed and then subjected to ethylenediaminetetraacetic acid (EDTA) antigen repair buffer (pH 8.0) in a microwave ovenated with bovine serum albumin. Sections were incubated with the Wilms tumor 1 (WT-1) antibody (1:100, Cat. Ab224806, Abcam, Cambridge, MA, USA), synaptopodin antibody (1:200, Cat. Ab259976, Abcam, Cambridge, MA, USA), nephrotic syndrome 2 (NPHS2) antibody (1:400, Cat. ab181143, Abcam, Cambridge, MA, USA), or nephrotic syndrome 1 (NPHS1) antibody (1:300, Cat. ab216341, Servicebio, Wuhan, China) overnight, followed by incubation with Fluorescein isothiocyanate (FITC)-conjugated goat anti-rabbit IgG (1:100, Cat. GB22303, Servicebio, Wuhan, China,) at room temperature for 50 min. Nuclei were counterstained with 4′,6-diamidino-2-phenylindole (DAPI). After slight drying, an autofluorescence quencher was applied for a water wash for 10 min. Finally, sections were securely sealed for subsequent analysis. DAPI-stained nuclei stained blue, and WT-1, synaptopodin, and NPHS2 stained green.

Journal of
BIOLOGICAL REGULATORS
and Homeostatic Agents

Table 1. Antibodies used in Western blot analysis.

Target	Dilution	Company	Cat. number
Dynamin-related protein 1 (Drp1)	1:2000	Abclonal, Wuhan, China	A2586
Mitofusin 1 (Mfn1)	1:2000	Abclonal, Wuhan, China	A9880
Cytochrome C (Cyto C)	1:2000	Abclonal, Wuhan, China	A4912
p-AMPK α1	1:1000	Abclonal, Wuhan, China	AP1002
AMPKα1	1:2000	Abclonal, Wuhan, China	A1229
SIRT1	1:2000	Abclonal, Wuhan, China	A11267
PGC-1α	1:1000	Abclonal, Wuhan, China	A12348
β-actin	1:50000	Abclonal, Wuhan, China	AC026

AMPK, AMP-activated protein kinase; SIRT1, silent information regulator sirtuin 1; PGC, peroxisome proliferator-activated receptor-gamma coactivator.

The acquired images were analyzed using Image J software (V1.6, National Institutes of Health, Bethesda, MD, USA) to measure the fluorescence intensity (IntDen) and area. Subsequently, the mean fluorescence intensity for each image was computed.

Detection of Intracellular Reactive Oxygen Species (ROS)

The ROS in renal tissues was quantified using a dichlorofluorescein diacetate (DCFH-DA) assay kit (Cat. S0033M; Beyotime Biotechnology, Shanghai, China). Briefly, renal tissues from each group of rats were obtained, sliced, and homogenized in normal saline (100 mg:1 mL). After centrifugation, the tissue supernatant was obtained and treated with 10 µM DCFH-DA at 37 °C for 20 min in the dark and then rinsed with phosphate-buffered saline and washing solution. Sections were detected by flow cytometry (Beckman Biomek FX, Beckman Coulter UK, High Wycombe, UK). After excitation at 488 nm wavelength, DCF emits a fluorescence signal at 525 mm wavelength, which is detected using the FITC channel.

Mitochondrial Membrane Potential (MMP)

The MMP of renal tissues was quantified utilizing the 5,5′,6,6′-tetrachloro-1,1′,3,3′-tetraethylbenzimidazolyl-carbocyanine iodide (JC-1) assay kit (Cat. C2003S; Beyotime Biotechnology, Shanghai, China). A diluted working solution of JC-1 was prepared by combining 900 µL of the diluted solution with 100 µL of purified mitochondria (approximately 100 µg post-purification). Subsequently, sections were incubated with 500 µL of 1× Incubation Buffer and analyzed utilizing flow cytometry (Beckman Biomek FX, Beckman Coulter, High Wycombe, UK). The flow cytometry results were analyzed using CxtLzpe software. MMP was estimated by measuring the ratio of red fluorescence (Q1-UR quadrant) to green fluorescence (Q1-LR quadrant).

Biochemical Assay

The levels of FBG, total cholesterol (TC), triglyceride (TG), serum albumin (ALB), creatinine (CREA), carbamide (UREA), alanine aminotransferase (ALT), and aspartate aminotransferase (AST) were analyzed using an automated biochemical device. Serum levels of fasting insulin were measured the Enzyme-Linked Immunosorbent Assay (ELISA) kit (Cat. ZC-37507, ZCIBIO, Shanghai, China), following the manufacturer's instructions. The homeostasis model assessment of insulin resistance (HOMA-IR) was calculated accordingly. The activity of superoxide dismutase (SOD; Cat. A001-3-1), glutathione-peroxidase (GSH-Px; Cat. A005-1-1), and malondialdehyde (MDA; Cat. A003-1-1) in renal tissues were evaluated using SOD, MDA, and GSH-Px detection kits, respectively (Nanjing Jiancheng Bioengineering Institute, Nanjing, China), following the manufacturer's protocols.

Real-Time Quantitative PCR (RT-qPCR) Assay

Total RNA was isolated from renal tissues using TRIzol® reagent (Cat. A33250, Thermo Fisher, Waltham, MA, USA). The RNA was reverse transcribed complementary DNA (cDNA) using a reverse transcription kit (Cat.4368813; Invitrogen, Carlsbad, CA, USA). RT-qPCR was conducted to determine the relative levels of target gene RNA transcripts using a SYBR Pemix Ex Taq kit (Cat. RR820A; Takara, Dalian, China). The reverse transcriptional reaction conditions were as follows: incubation at 95 °C for 30 s, followed by 40 cycles of incubation at 95 °C for 5 s, and then at 60 °C for 30 s. The $2^{-\Delta\Delta Ct}$ method was applied to calculate relative gene expression levels using ABI software (Prism 7500, ABI, Foster City, CA, USA). The sequences of RT-qPCR primers were as follows. AMP-activated protein kinase (*AMPK*): forward primer, 5′-CGATGATGAGGTGGTGGAGCAGAGGT-3′; reverse primer, 5′-GTGAATGGTTCTCGGCTGTGCTGGAA-3′, 232 bp; peroxisome proliferator-activated receptor-gamma coactivator (*PGC*)-*1*α: forward primer, 5′-CCTCACACCAAACCCACAGAGAAC-3′; reverse primer, 5′-TTGCGACTGCGGTTGTGTATGG-3′, 232 bp; silent information regulator sirtuin 1 (*SIRT1*): forward primer, 5′-TGGCAGTAACAGTGACAGTGGCACAT-3′; reverse primer, 5′-TCAGCTCCAGATCCTCCAGCACACTC-

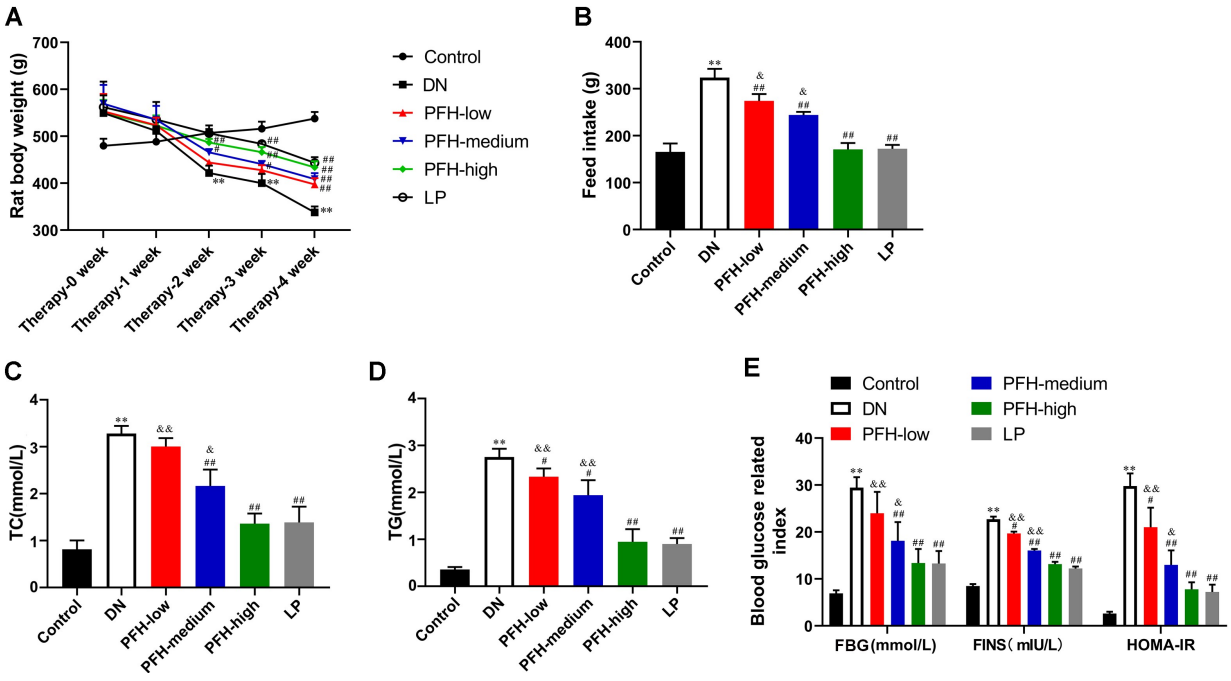

Fig. 1. PFH improved metabolic abnormalities in diabetic rats. (A) Weekly changes in rat weight. (B) The average food intake by the rats during the last week (total food intake of 6 rats in each group). The serum level of total cholesterol (TC, C), triglyceride (TG, D), fasting blood glucose (FBG, E), and fasting insulin levels (FINS, E) after 12 h of fasting. $^{**}p < 0.01$ vs. control group. $^{\#}p < 0.05$ vs. Diabetic nephropathy (DN) model group. $^{\#\#}p < 0.01$ vs. DN group. $^{\&}p < 0.05$ vs. Losartan Possaium (LP) group. $^{\&\&}p < 0.01$ vs. LP group. n = 6. PFH, Polygala fallax Hemsl. PFH-low, low-dose PFH group; PFH-medium, medium-dose PFH group; PFH-high, high-dose PFH group; LP, Losartan Potassium; HOMA-IR, homeostasis model assessment of insulin resistance.

3′; *β-actin*: forward primer, 5′-GGGAAATCGTGCGTGACATT-3′; reverse primer, 5′-GCGGCAGTGGCCATCTC-3′.

Western Blot Analysis

The radioimmunoprecipitation (RIPA) assay buffer (Cat. 9806, Cell Signaling Technologies, Inc., Danvers, MA, USA) was used to extract all proteins from renal tissues, and the bicinchoninic acid (BCA) kit (Cat. P0009; Biyuntian Biotechnology Co., Ltd., Shanghai, China) was utilized for protein quantification. Based on the quantitative results, a loading volume of 20 μg per well was utilized for spot sampling, and the total protein was separated through 10% sodium dodecyl-sulfate polyacrylamide gel electrophoresis (SDS-PAGE). Afterward, the membrane was transferred to Immobilon-PSQ polyvinylidene fluoride (PVDF) membrane (Cat. ISEQ00010; Sigma-Aldrich, St. Louis, MO, USA), blocked with 5% skim milk, and incubated with an appropriate amount of primary antibody at 4 °C overnight. After washing with Tris-buffered saline + 0.1% Tween (TBST), the membrane was incubated with a horseradish peroxidase-conjugated goat anti-rabbit IgG (heavy and light chains) secondary antibody (1/5000, Cat. S0001, Affbiotech, Cincinnati, OH, USA) at room temperature for 2 h. Finally, the ECL color development solution was utilized for chromogenic detection. The bands were detected using the Tanon fluorescent image analysis system software V2.0 (Tanon, Shanghai, China), and the resulting exposure data were scanned using Gel-Pro analyzer4 software (Atto, Tokyo, Japan) and quantified as an integrated optical density (IOD) of the target protein. Relative protein expression was calculated. The primary antibodies utilized for Western blot were shown in (Table 1).

Statistical Analysis

Data were expressed as mean ± standard deviation. Data were analyzed using SPSS 22.0 software (IBM Corp., Armonk, NY, USA). One-way analysis of variance (ANOVA) was used to compare the differences between the means of more than two groups. The level of statistical significance was set at $p < 0.05$.

Results

Analysis of PFH Active Ingredients

UPLC-MS was used to evaluate the chemical composition of PFH. In the chromatographic profile of PFH, 3,4-dihydroxymandelic acid, Tryptophol, Convallatoxin, 10-hydroxyusambarine, and 3,3′,4′,7-tetrahydroxyflavylium chloride were detected in the positive ionization scan mode (**Supplementary Fig. 1**), whereas 11-(3,5-disulfooxyphenyl) undecan-4-

Journal of
BIOLOGICAL REGULATORS
and Homeostatic Agents

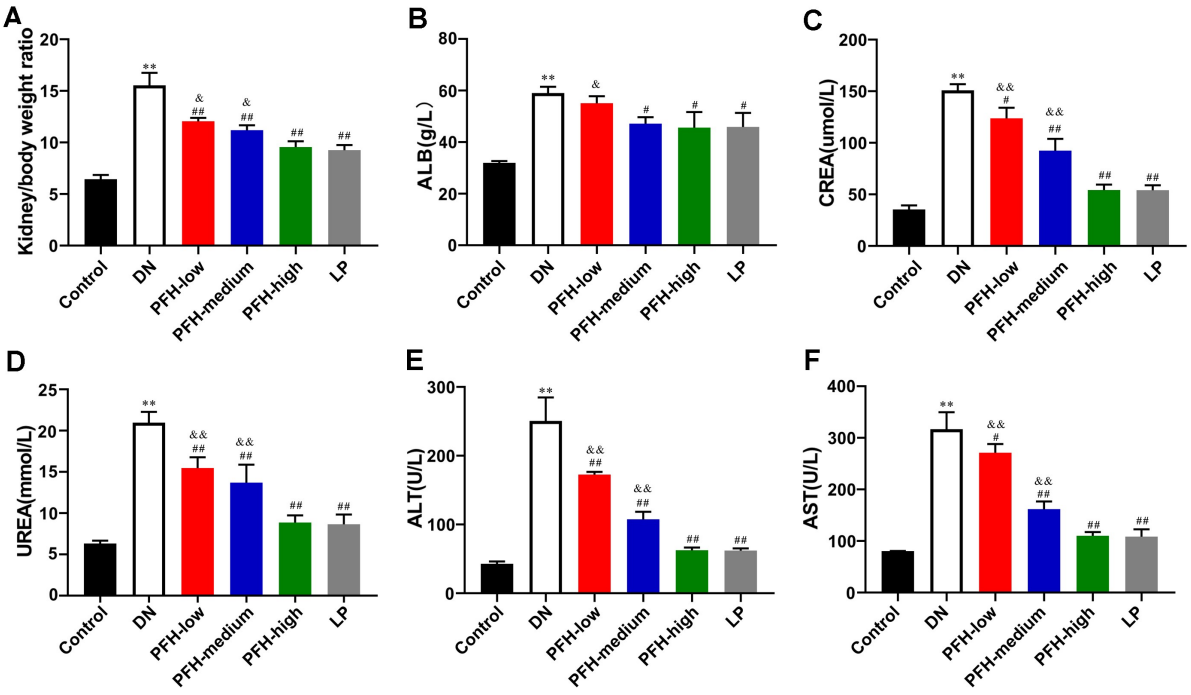

Fig. 2. PFH treatment improves renal function in diabetic rats. (A) The kidney index indicates kidney hypertrophy as calculated based on the kidney weight/body weight (mg/g). (B) Serum albumin (ALB), (C) creatinine (CREA), (D) carbamide (UREA), (E) alanine aminotransferase (ALT), and (F) aspartate aminotransferase (AST) was detected using the biochemical analyzer. $^{**}p < 0.01$ vs. control group. $^{\#}p < 0.05$ vs. Diabetic nephropathy (DN) model group. $^{\#\#}p < 0.01$ vs. DN group. $^{\&}p < 0.05$ vs. Losartan Possaium (LP) group. $^{\&\&}p < 0.01$ vs. LP group. n = 6.

yl 3,5-dihydroxy-2-undecylbenzoate, verruculotoxin, pentadecafluoroheptan-1-ol, 5-aminonaphthalene-2-sulfonic acid, and Ochrephilone were detected in the negative ionization scan mode (**Supplementary Fig. 1**). The identification of PFH active substances is shown in **Supplementary Table 1**.

PFH Ameliorates Metabolic Abnormalities in Diabetic Rats

After 4 weeks of treatment, weekly rat weight measurements showed that compared with the DN group, PFH and LP treatments gradually increased the body weight in diabetic rats (Fig. 1A; $p < 0.05$ or $p < 0.01$). Meanwhile, PFH and LP treatments decreased food intake on the fourth week of treatment ($p < 0.01$). In addition, the degree of improvement of PFH increased with the increase in concentration (Fig. 1B). Compared with the control group, TC, TG, FBG, fasting insulin levels (FINS), and HOMA-IR levels were elevated in untreated diabetic rats (Fig. 1C–E; $p < 0.01$). However, rats treated with different concentrations of PFH and LP showed a decreasing trend of TC, TG, FBG, FINS, and HOMA-IR levels compared with diabetic rats (Fig. 1C–E; $p < 0.05$ or $p < 0.01$).

PFH Treatment Improves Renal Function and Renal Tissue Injury in Diabetic Rats

The diabetic rat group exhibited a marked rise in the kidney hypertrophy index (Fig. 2A; $p < 0.01$). Treatment of STZ-diabetic rats with PFH doses of 2, 4, and 8 g/kg ameliorated the kidney hypertrophy index (Fig. 2A; $p < 0.01$). Serum levels of ALB, CREA, UREA, ALT, and AST were higher in the DN model group than in the control group (Fig. 2B–F; $p < 0.01$). Treatment with different concentrations of PFH and LP significantly decreased serum levels of ALB, CREA, UREA, ALT, and AST (Fig. 2B–F; $p < 0.05$ or $p < 0.01$). H&E staining revealed renal tubular epithelial cell swelling, glomerular hypercellularity, and an increase in basement membrane thickness in the DN group (Fig. 3A). PFH treatment reduced renal tissue injury and neutrophil infiltration (Fig. 3A). The effect of PFH was consistent with positive drug action, with the high-dose group exhibiting the most significant effect (Fig. 3A). PAS-stained renal sections showed glomerular cluster leaf protrusion and mesangial hyperplasia in diabetic rats, which was decreased by medium- and high-dose PFH and LP treatments (Fig. 3B,C; $p < 0.01$). Additionally, Masson's trichrome staining exhibited heightened levels of glomerular and tubule-interstitial fibrosis in the kidneys of diabetic rats (Fig. 3D,E; $p < 0.01$). Treatment with different concentrations of PFH and LP decreased the content of collagen fibers (Fig. 3D,E; $p < 0.01$).

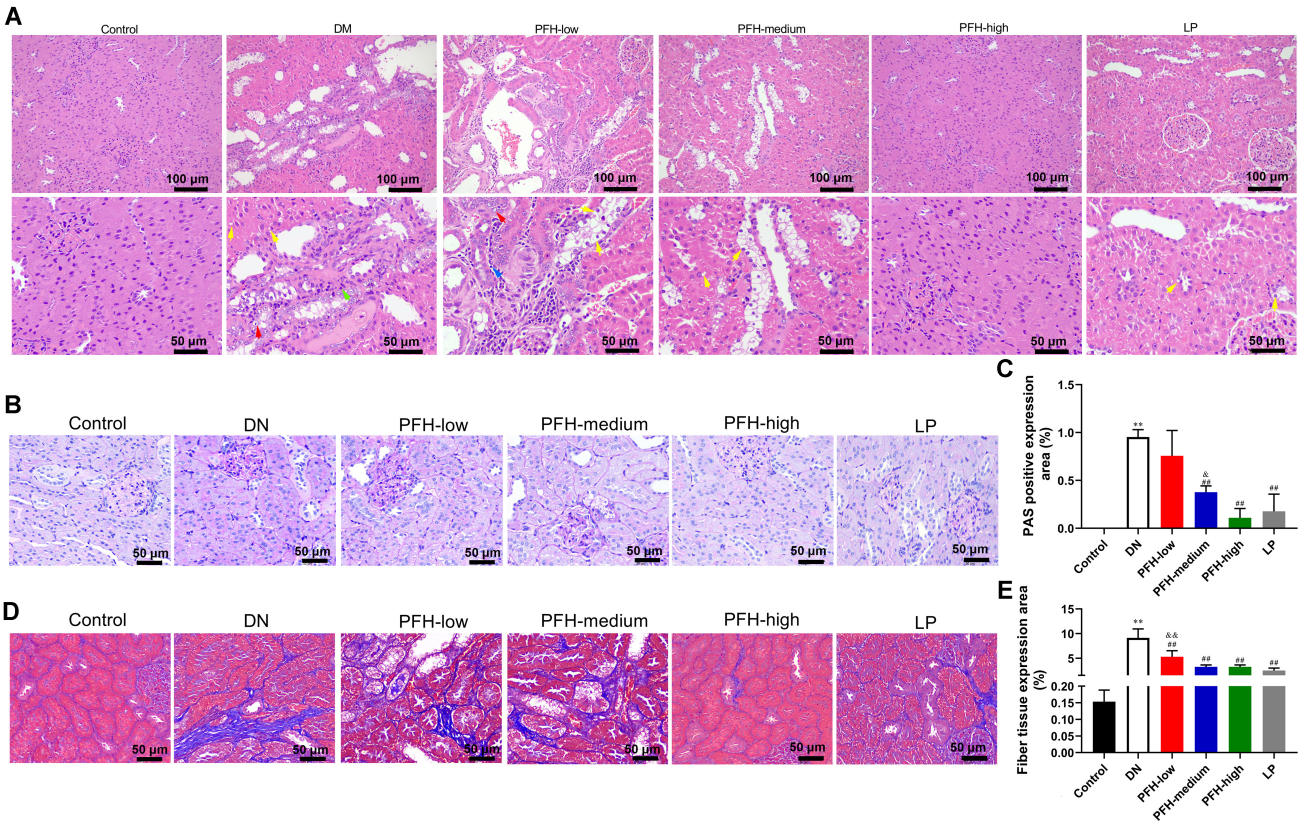

Fig. 3. PFH treatment improves renal tissue injury in diabetic rats. (A) Hematoxylin-eosin (H&E) staining was conducted to evaluate kidney histopathology. Yellow arrow indicates renal tubular epithelial cell degeneration; Green arrow shows the neutrophils; Red arrow indicates renal tubular epithelial cell swelling; Blue arrow represents lymphocytes. Magnification, 200× and 400×. Scale bar, 50 μm. (B) Periodic acid-Schiff (PAS) staining of renal tissue to examine the glomerular and tubular basement membrane. Magnification, 400×. Scale bar, 50 μm. (C) The percentage of PAS-positive cells was calculated. (D,E) The area of fibrosis was determined using a Masson trichrome staining method. Magnification, 400×. Scale bar, 50 μm. $^{**}p < 0.01$ vs. control group. $^{\#\#}p < 0.01$ vs. Diabetic nephropathy (DN) model group. $^{\&}p < 0.05$ vs. Losartan Possaium (LP) group. $^{\&\&}p < 0.01$ vs. LP group. n = 6.

PFH Treatment Reduces Renal Podocyte Mitochondrial Dysfunction in Diabetic Rats

Compared with the control group, GSH-Px and SOD levels were dramatically reduced (Fig. 4A; $p < 0.01$) and the level of MDA was significantly increased in the renal tissue of diabetic rats (Fig. 4A; $p < 0.01$). However, PFH and LP treatment reversed these effects. In addition, the mitochondrial dynamic status was assessed by measuring Dynamin-related protein 1 (Drp1), Mitofusin 1 (Mfn1), and Cytochrome C (Cyto C) protein expression levels (Fig. 4B,C). The renal tissue of diabetic rats exhibited a marked elevation in the expression levels of Drp1 and Cyto C (Fig. 4B,C; $p < 0.01$). However, the expression level of Mfn1 decreased significantly in the DN group compared with the control group (Fig. 4B,C; $p < 0.01$). Drp1 and Cyto C protein expression levels decreased dramatically in the low-/medium-/high-dose PFH or LP treatment group (Fig. 4B,C; $p > 0.05$, $p < 0.05$, or $p < 0.01$). Moreover, the Mfn1 expression level was significantly increased after PFH or LP treatment (Fig. 4B,C; $p < 0.05$, or $p < 0.01$). The MMP was significantly decreased in the DN model ($p < 0.01$), which was reversed by PFH and LP treatments (Fig. 4D,E; $p < 0.05$ or $p < 0.01$). Meanwhile, ROS levels were significantly increased in the renal tissue of diabetic rats (Fig. 4F,G; $p < 0.01$). ROS levels were reduced in the low-, medium-, and high-dose PFH treatment groups and the LP treatment group (Fig. 4F,G; all $p < 0.01$). Glomerular TEM images showed that the degree of mitochondrial swelling, vacuolation, and crest fragmentation in the podocytes of diabetic rat kidney sections was increased, which was attenuated by PFH and LP treatments (Fig. 4H).

PFH Treatment Alleviates Podocyte Injury in Diabetic Rats

IHC staining results indicated that the protein expression of caspase-3 was significantly elevated in diabetic rats compared with the control group (Fig. 5A,B; $p < 0.01$). The PFH or LP-treated group showed no significant alteration in caspase-3 expression (Fig. 5A,B; $p > 0.05$). In addition, STZ induction significantly elevated cleaved-caspase-3 ex-

Journal of
BIOLOGICAL REGULATORS
and Homeostatic Agents

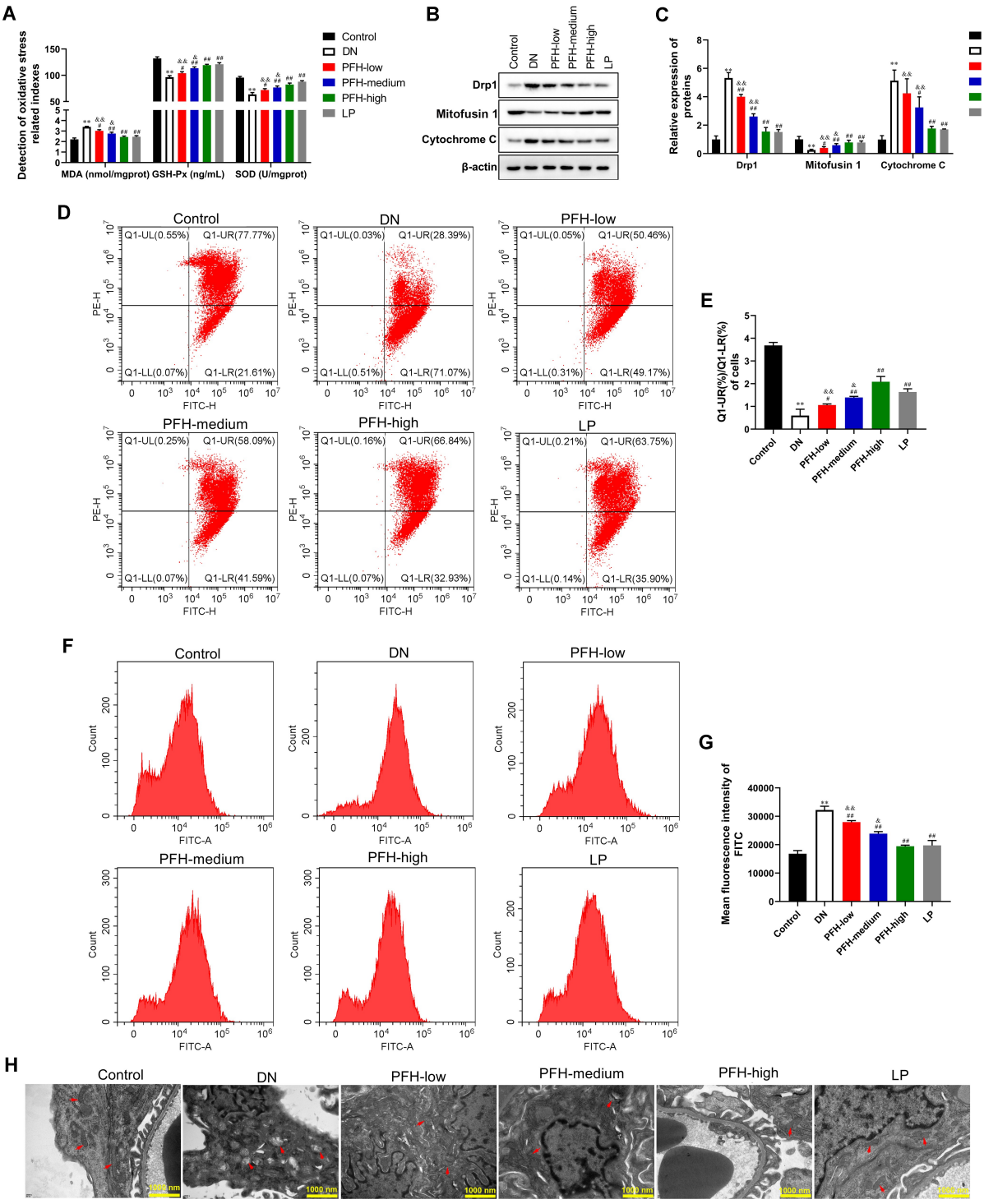

Fig. 4. PFH treatment reduced renal podocyte mitochondrial dysfunction in diabetic rats. (A) The concentration of malondialdehyde (MDA), glutathione-peroxidase (GSH-Px), and superoxide dismutase (SOD) in rat renal tissue as detected using a biochemical kit. (B,C) The protein expression of Drp1, Mfn1, and Cyto C in rat renal tissues was quantified by Western blot. β-actin served as the internal reference protein. (D,E) The mitochondrial membrane potential (MMP) of rat renal tissue was measured with a JC-1 mitochondrial staining kit. (F,G) The dichlorofluorescin diacetate (DCFDA) assay was conducted to determine the production of reactive oxygen species (ROS) in rat renal tissues. (H) The morphology of renal mitochondria was examined using a transmission electron microscope (TEM). Red arrow, mitochondrial degeneration. Scale bar, 1000 nm. $^{**}p < 0.01$ vs. control group. $^{\#}p < 0.05$ vs. Diabetic nephropathy (DN) model group. $^{\#\#}p < 0.01$ vs. DN group. $^{\&}p < 0.05$ vs. Losartan Possaium (LP) group. $^{\&\&}p < 0.01$ vs. LP group. n = 6. FITC, Fluorescein isothiocyanate.

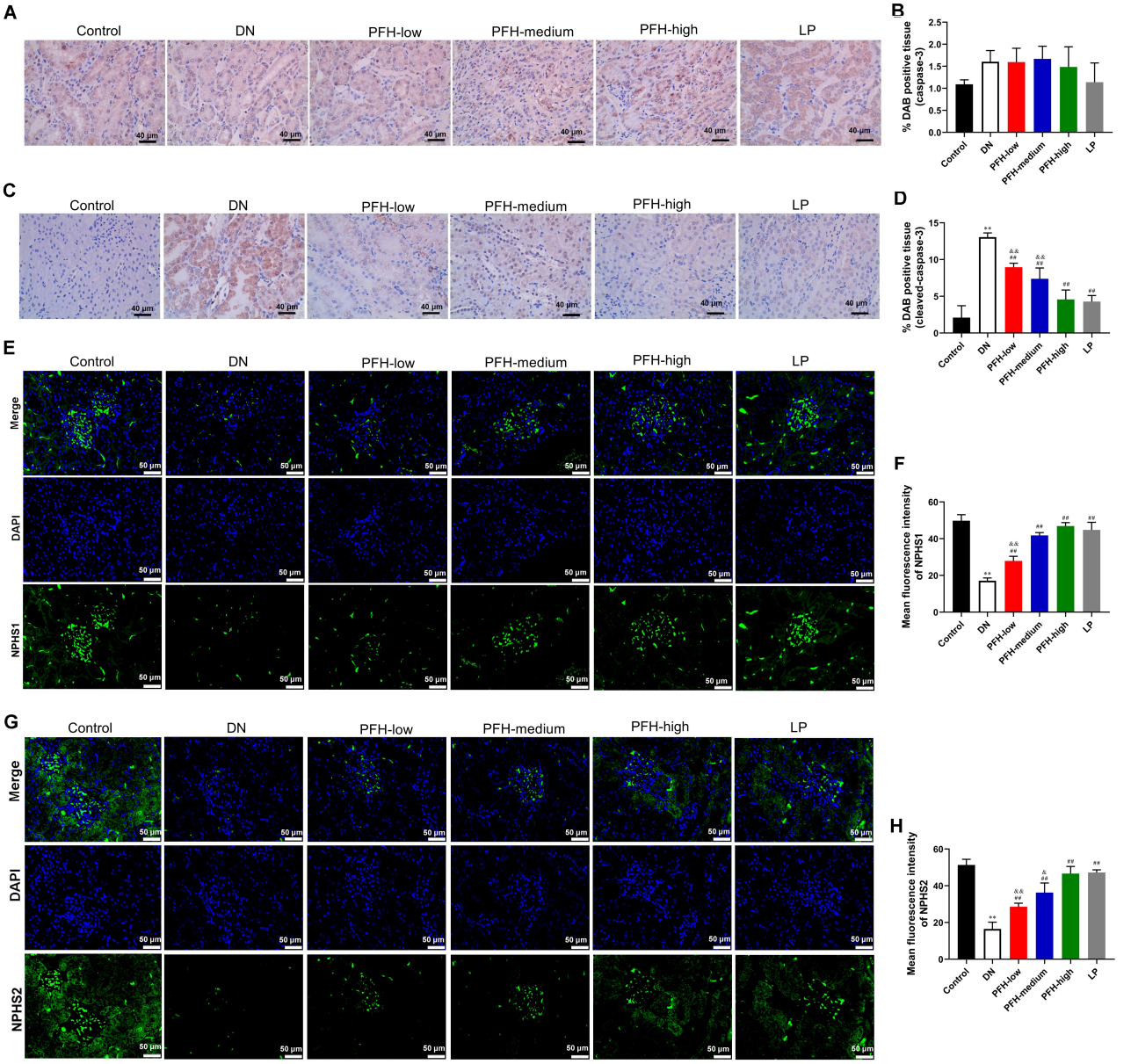

Fig. 5. PFH treatment alleviated podocyte injury in diabetic rats. The immunohistochemistry (IHC) staining technique was utilized to measure the existence of caspase-3 (A,B) and cleaved-caspase-3 (C,D) in renal tissue samples from rats. The images were recorded at a magnification of 400×, with a scale bar measuring 40 μm. Immunofluorescent (IF) staining was utilized to assess the expression of nephrotic syndrome 1 (NPHS1) (E,F) and nephrotic syndrome 2 (NPHS2). (G,H) in rat renal tissue. The images were taken at a magnification of 400×, with a scale bar measuring 50 μm. $^{**}p < 0.01$ vs. control group. $^{\#\#}p < 0.01$ vs. Diabetic nephropathy (DN) model group. $^{\&}p < 0.05$ vs. Losartan Possaium (LP) group. $^{\&\&}p < 0.01$ vs. LP group. n = 6. DAB, 3,3′-diaminobenzidine; DAPI, 4′,6-diamidino-2-phenylindole.

pression levels compared with the control group (Fig. 5C,D; $p < 0.01$). PFH or LP intervention significantly inhibited the expression of cleaved-caspase-3 (Fig. 5C,D; $p < 0.01$). PFH improvement showed a concentration-dependent trend (Fig. 5C,D). IF staining revealed that protein expression of podocyte markers NPHS1 and NPHS2 was most strongly downregulated in the renal tissue of diabetic rats (Fig. 5E–H; $p < 0.01$). Consistently, PFH dose-dependently increased the expression of NPHS1 and NPHS2 (Fig. 5E–H; $p < 0.01$). Treatment with a high dosage of PFH exhibited a comparable influence on the expression levels of NPHS1 and NPHS2, akin to the positive effects observed with LP, a well-recognized medication (Fig. 5E–H).

In addition, the glomerulus was subjected to double IF staining of synaptopodin and WT-1 proteins, which are specific markers for podocyte cells, to validate their expression. The results revealed a dramatic decline in the expression levels of synaptopodin and WT-1 in the renal tis-

Journal of
BIOLOGICAL REGULATORS
and Homeostatic Agents

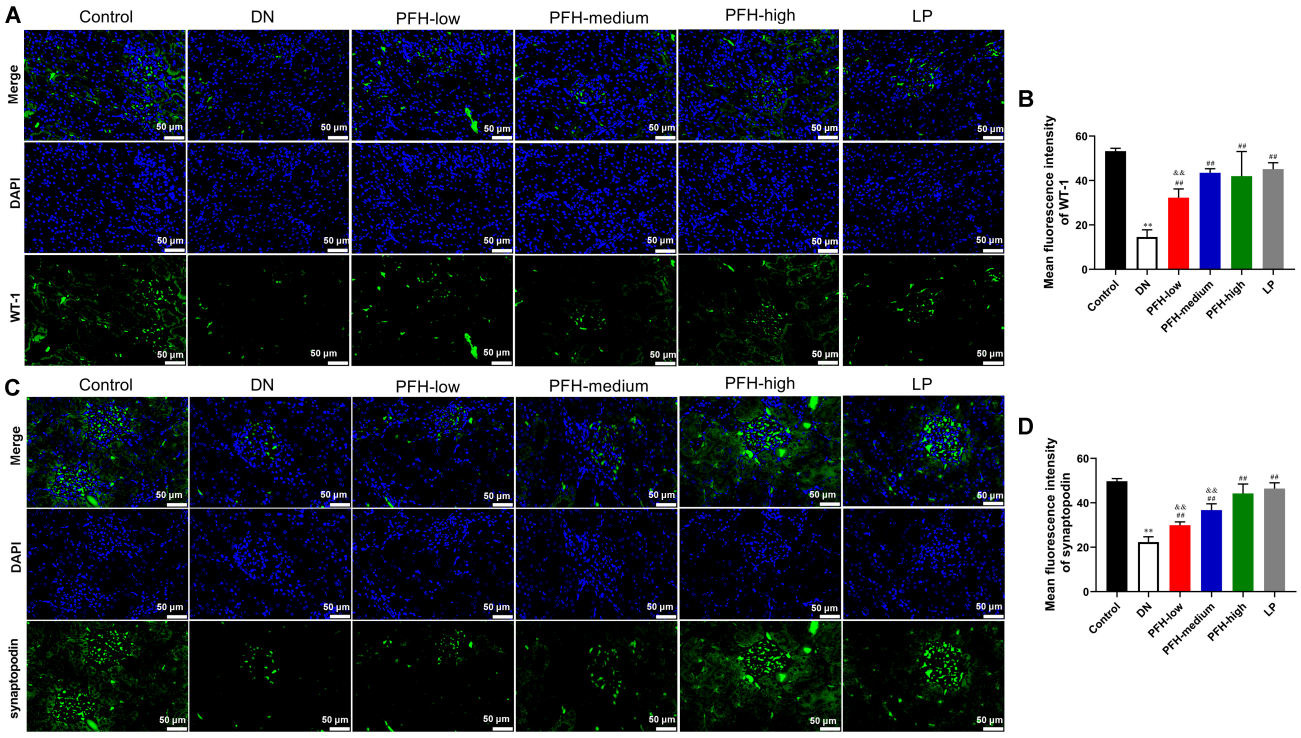

Fig. 6. Receiving PFH treatment resulted in increased levels of Wilms tumor 1 (WT-1) and synaptopodin expression in rats with diabetes. The expression level of WT-1 (A,B) and synaptopodin (C,D) in renal tissues of rats was detected by immunofluorescence. Magnification, 400×. Scale bar, 50 μm. $^{**}p < 0.01$ vs. control group. $^{\#\#}p < 0.01$ vs. Diabetic nephropathy (DN) model group. $^{\&\&}p < 0.01$ vs. LP group. n = 6.

sue of diabetic rats (Fig. 6A–D; $p < 0.01$). PFH and LP treatment reduced the fluorescence intensities of podocyte injury markers synaptopodin and WT-1 (Fig. 6A–D; $p < 0.01$). The high-dose PFH group exhibited the most pronounced therapeutic effect (Fig. 6A–D; $p < 0.01$).

PFH Treatment Promotes the AMPK/SIRT1/PGC-1α Signaling Pathway in the Renal Tissue of Diabetic Rats

The expression of proteins involved in AMP-activated protein kinase (AMPK)/silent information regulator sirtuin 1 (SIRT1)/peroxisome proliferator-activated receptor-gamma coactivator-1α (PGC-1α) signaling was assessed in STZ-induced diabetic rats *in vivo*. The results showed that the activity of the AMPK/SIRT1/PGC-1α signaling pathway was decreased in renal tissues of diabetic rats, which was manifested by significantly decreased protein expression levels of phosphorylated AMPK (p-AMPK) (Fig. 7A,D,F; $p < 0.01$), as well as decreased mRNA and protein expression levels of SIRT1 and PGC-1α (Fig. 7B,C,E,F,H; $p < 0.01$). Furthermore, RT-qPCR results revealed that PFH or LP intervention significantly increased mRNA levels of *SIRT1* and *PGC-1α*; however, mRNA levels of *AMPK* were not significantly altered (Fig. 7A–H; $p > 0.05$, $p < 0.05$, or $p < 0.01$). Western blot analysis was also performed to detect the protein expression of p-AMPK, SIRT1, and PGC-1α, and the results showed that protein levels of these molecules were significantly increased after PFH or LP treatment (Fig. 7A–H; $p < 0.05$ or $p < 0.01$). Meanwhile, the PFH therapy dose-dependently activated the AMPK/SIRT1/PGC-1α signaling pathway (Fig. 7A–H; $p < 0.05$ or $p < 0.01$).

Discussion

PFH extract is a pharmaceutical compound with demonstrated anti-inflammatory, anti-tumor, and other pharmacological effects [13,15]. However, its mechanism of action in DN remains unclear. The present study found that ALB, CREA, and UREA levels were significantly reduced in diabetic rats compared with normal rats after PFH treatment, indicating significant pharmacodynamic effects. Morphologically, renal tissue was assessed using H&E, PAS, and Masson's trichrome staining techniques. The presence of inflammatory cell infiltration was detected within certain glomerular renal tubules in the diabetic rat model, which was accompanied by the thickening of the glomerular basement membrane and denaturation of renal tubule epithelial cells. Moreover, treatment with PFH significantly ameliorated these pathological changes.

The mitochondrial injury occurring in the podocyte represents a distinctive characteristic in the progression of DN [6,17]. Podocytes maintain their structure and function by regulating cytoskeletal proteins and the extracellular

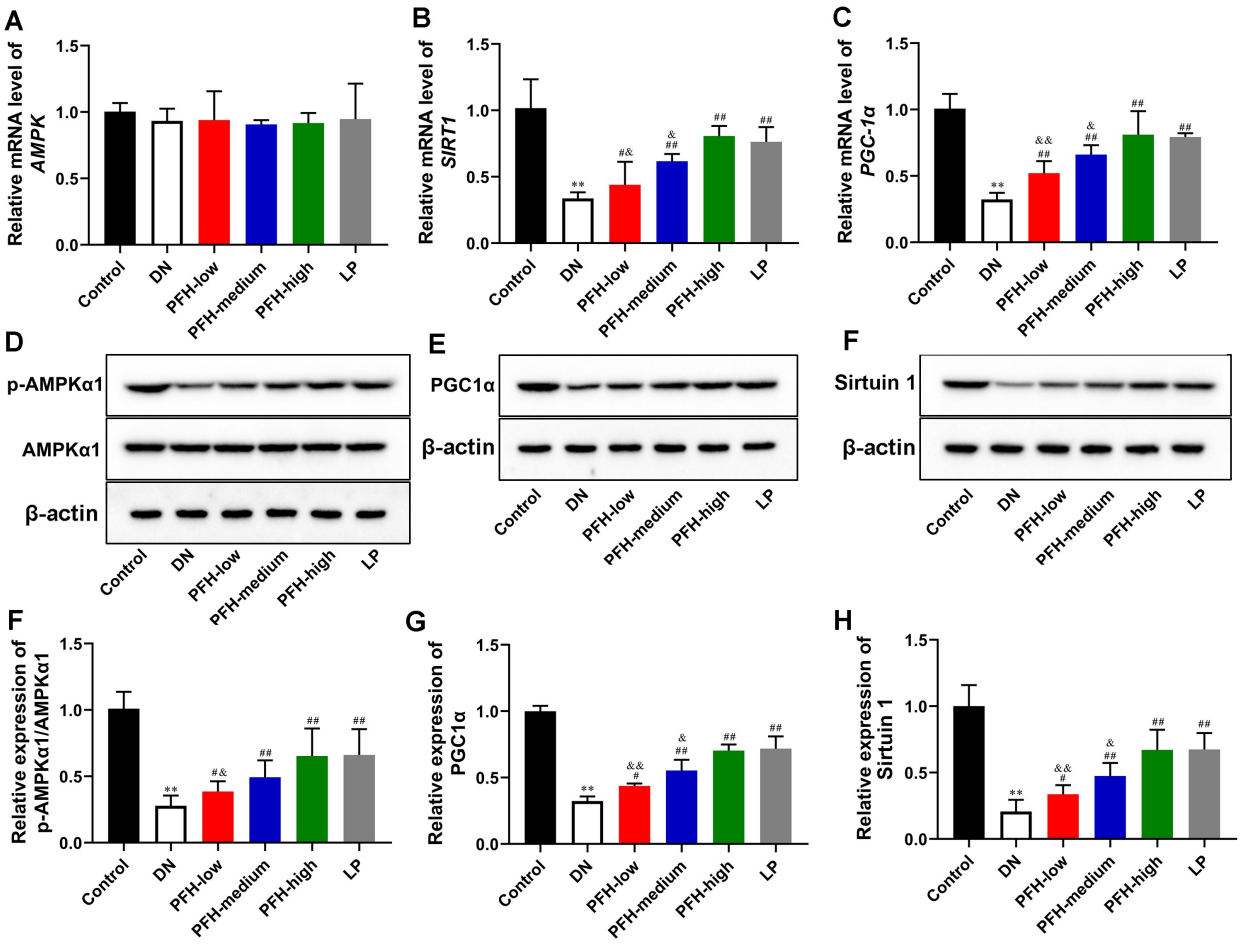

Fig. 7. PFH treatment promoted AMPK/SIRT1/PGC-1α signaling pathway activity in renal tissue of diabetic rats. (A–C) Real-time quantitative PCR (RT-qPCR) was performed to measure the mRNA expression levels of *AMPK*, *SIRT1*, and *PGC-1α* in rat renal tissue. (D–H) The protein expression levels of p-AMPK, AMPK, SIRT1, and PGC-1α in rat renal tissue were measured by Western blot. *β-actin* served as the reference gene. $^{**}p < 0.01$ vs. control group. $^{\#}p < 0.05$ vs. Diabetic nephropathy (DN) model group, $^{\#\#}p < 0.01$ vs. DN group. $^{\&}p < 0.05$ vs. Losartan Potassium (LP) group. $^{\&\&}p < 0.01$ vs. LP group. n = 6. p-AMPK, phosphorylated AMPK.

matrix, and this process requires a sufficient energy supply [18]. Mitochondria are the energy supply sites for the vital activities of podocytes and also participate in the regulation of cell metabolism, cell proliferation, programmed cell death, calcium homeostasis, and other processes [19,20]. When podocytes are stimulated by HG, the structure and function of mitochondria will change, resulting in mitochondrial dysfunction and damage, ultimately leading to podocyte injury [21–23]. In addition, excessive fragmentation of the mitochondria has been observed in podocytes of animal models with DN [24,25]. The excessive occurrence of mitochondrial fission plays a crucial role in triggering the production of ROS and proteins associated with apoptosis, ultimately leading to the initiation of the mitochondrial apoptotic pathway [26,27]. Therefore, to maintain the balance of podocytes, it is necessary to eliminate dysfunctional mitochondria. Several traditional Chinese medicine components have demonstrated their potential in improving mitochondrial impairment in podocytes. Berberine resulted in notable improvements in glucose and lipid metabolism disorders, as well as podocyte damage. Additionally, it exhibited inhibitory effects on mitochondrial fragmentation and dysfunction by positively modulating Drp1-mediated mitochondrial dynamics [28]. Ginsenoside Rb1 combined with aldose reductase reduced HG-induced podocyte apoptosis and mitochondrial damage and effectively delayed the progression of DN [29]. Moreover, resveratrol mitigated podocyte injury in diabetic mice through SIRT1/PGC-1α-mediated mitigation of mitochondrial oxidative stress [30]. Our findings demonstrated that PFH treatment inhibited podocyte apoptosis, increased ROS generation, and triggered mitochondrial fragmentation and impairment in the renal system of diabetic rats.

The AMPK, SIRT1, and PGC-1α signaling pathways play a crucial role in sensing energy levels [31,32]. Different metabolic processes, including glucose metabolism, protein metabolism, and cell cycle regulation, are controlled by AMPK [33]. The activity of AMPK is regu-

Journal of
BIOLOGICAL REGULATORS
and Homeostatic Agents

lated by the adenosine monophosphate (AMP)/adenosine triphosphate (ATP) ratio, which has become an important factor in regulating energy metabolism [34]. Blood glucose balance is significantly regulated by AMPK [35,36]. Previous studies suggested that AMPK activation can change the nicotinamide adenine dinucleotide (NAD)/nicotinamide adenine dinucleotide (NADH) ratio, thereby activating SIRT1 [37]. Further, the AMPK/SIRT1 pathway plays a crucial role in mitochondrial biosynthesis and energy metabolism [38,39]. SIRT1 has been implicated in the pathogenesis of diabetes and other disorder [40,41]. Overexpression of SIRT1 has been shown to exert preventive and therapeutic effects on DN [42,43]. AMPK and SIRT1 interact with each other and share several common target molecules, such as PGC-1α [44]. PGC-1α enhancing ATP levels thereby significantly reducing oxidative stress-induced ROS production and cell apoptosis [45]. This study provides evidence that glycyrrhizin acid-mediated AMPK activation, SIRT1, and PGC-1α can mitigate renal lipid accumulation and cellular damage [46]. The findings suggest that glycyrrhizin activates the AMPK/SIRT1/PGC-1α signaling, which is typically inhibited in diabetes [46]. Moreover, the results suggest a reciprocal activation mechanism between AMPK and SIRT1, involving coordinated regulation of their common downstream effector, PGC-1α, in glomerular mesangial cells [47]. The administration of a polysaccharide extracted from okra significantly improved Diabetic nephropathy by inhibiting apoptosis and alleviating oxidative stress through the amplification of the AMPK/SIRT1/PGC-1α axis [48]. 5-aminoimidazole-4-carboxamide-1-riboside (AICAR) [49] or adiponectin [50] suppressed oxidative stress and apoptosis via activating the AMPK signaling, thereby reducing renal podocyte injury and proteinuria in diabetic animals. Grape seed procyanidin B2 protected podocytes from mitochondrial dysfunction and apoptosis induced by high glucose via the AMPK/SIRT1/PGC-1α pathway *in vitro* [51]. Similarly, our findings indicate that PFH may ameliorate mitochondrial dysfunction of podocytes in Diabetic nephropathy by activating the AMPK/SIRT1/PGC-1α signaling pathway in renal tissue of diabetic rats.

The major limitation of this study is that the effect of PFH on other factors has not been studied, such as different types of diabetes, disease course, and complications, which are important factors affecting its clinical applicability. Moreover, more studies are needed to dissect the role of PFH in DN and its safe dose for clinical use, including studies using different animal models of DN.

Conclusion

This study demonstrates that PFH can ameliorate renal impairment and alleviate oxidative damage to podocyte mitochondria in diabetic rats via activating the AMPK/SIRT1/PGC-1α signaling pathway. Therefore, PFH holds promise as a potential pharmaceutical intervention for the protection and prevention of diabetic nephropathy.

Availability of Data and Materials

The datasets used or analyzed during the current study are available from the corresponding author on reasonable request.

Author Contributions

SC designed the research study. SC, YY, WC, and HT performed the research. BC provided help and advice on the TEM experiments. SC and YY analyzed the data. All authors contributed to editorial changes in the manuscript. All authors read and approved the final manuscript. All authors have participated sufficiently in the work and agreed to be accountable for all aspects of the work.

Ethics Approval and Consent to Participate

The study protocols were approved by the Ethics Committee of Guilin Hospital of the Second Xiangya Hospital Central South University (No. 20210710).

Acknowledgment

Not applicable.

Funding

This work was supported by the National Natural Science Foundation of China under Grant [number 82160802].

Conflict of Interest

The authors declare no conflict of interest.

Supplementary Material

Supplementary material associated with this article can be found, in the online version, at https://doi.org/10.23812/j.biol.regul.homeost.agents.20243805.344.

References

[1] Samsu N. Diabetic Nephropathy: Challenges in Pathogenesis, Diagnosis, and Treatment. BioMed Research International. 2021; 2021: 1497449.

[2] Umanath K, Lewis JB. Update on Diabetic Nephropathy: Core Curriculum 2018. American Journal of Kidney Diseases: the Official Journal of the National Kidney Foundation. 2018; 71: 884–895.

[3] Li X, Lu L, Hou W, Huang T, Chen X, Qi J, *et al*. Epigenetics in the pathogenesis of diabetic nephropathy. Acta Biochimica et Biophysica Sinica. 2022; 54: 163–172.

[4] McGowan T, McCue P, Sharma K. Diabetic nephropathy. Clinics in Laboratory Medicine. 2001; 21: 111–146.

[5] Bonner R, Albajrami O, Hudspeth J, Upadhyay A. Diabetic Kidney Disease. Primary Care. 2020; 47: 645–659.
[6] Barutta F, Bellini S, Gruden G. Mechanisms of podocyte injury and implications for diabetic nephropathy. Clinical Science (London, England: 1979). 2022; 136: 493–520.
[7] Bose M, Almas S, Prabhakar S. Wnt signaling and podocyte dysfunction in diabetic nephropathy. Journal of Investigative Medicine: the Official Publication of the American Federation for Clinical Research. 2017; 65: 1093–1101.
[8] Dai H, Liu Q, Liu B. Research Progress on Mechanism of Podocyte Depletion in Diabetic Nephropathy. Journal of Diabetes Research. 2017; 2017: 2615286.
[9] Liu XJ, Hu XK, Yang H, Gui LM, Cai ZX, Qi MS, *et al*. A Review of Traditional Chinese Medicine on Treatment of Diabetic Nephropathy and the Involved Mechanisms. The American Journal of Chinese Medicine. 2022; 50: 1739–1779.
[10] Sun GD, Li CY, Cui WP, Guo QY, Dong CQ, Zou HB, *et al*. Review of Herbal Traditional Chinese Medicine for the Treatment of Diabetic Nephropathy. Journal of Diabetes Research. 2016; 2016: 5749857.
[11] Yao Z, Li Y, Wang Z, Lan Y, Zeng T, Gong H, *et al*. Research on anti-hepatocellular carcinoma activity and mechanism of Polygala fallax Hemsl. Journal of Ethnopharmacology. 2020; 260: 113062.
[12] Chao S, Xu Q, Dong S, Guo M, Liu X, Cheng X. *Polygala fallax* Hemsl combined with compound Sanqi granules relieves glomerulonephritis by regulating proliferation and apoptosis of glomerular mesangial cells. The Journal of International Medical Research. 2020; 48: 300060519894124.
[13] Yang G, Lang Y. Extract identification and evaluation of the cytotoxic activity of Polygala fallax Hemsl in Heilongjiang ethnic medicine against tumors. Technology and Health Care: Official Journal of the European Society for Engineering and Medicine. 2023; 31: 565–575.
[14] Zhong C, Ju G, Yang S, Zhao X, Chen J, Li N. Total Flavonoids of Polygala fallax Hemsl Induce Apoptosis of Human Ectopic Endometrial Stromal Cells through PI3K/AKT/Bcl-2 Signaling Pathway. Gynecologic and Obstetric Investigation. 2023; 88: 197–213.
[15] Wang M, Liu X, Wang Z, Xu Q. The extract of Polygala fallax Hemsl. slows the progression of diabetic nephropathy by targeting TLR4 anti-inflammation and MMP-2/9-mediated anti-fibrosis in vitro. Phytomedicine: International Journal of Phytotherapy and Phytopharmacology. 2022; 104: 154251.
[16] Rigby MR, Trexler AM, Pearson TC, Larsen CP. CD28/CD154 blockade prevents autoimmune diabetes by inducing nondeletional tolerance after effector t-cell inhibition and regulatory T-cell expansion. Diabetes. 2008; 57: 2672–2683.
[17] Liu S, Yuan Y, Xue Y, Xing C, Zhang B. Podocyte Injury in Diabetic Kidney Disease: A Focus on Mitochondrial Dysfunction. Frontiers in Cell and Developmental Biology. 2022; 10: 832887.
[18] Denhez B, Rousseau M, Dancosst DA, Lizotte F, Guay A, Auger-Messier M, *et al*. Diabetes-Induced DUSP4 Reduction Promotes Podocyte Dysfunction and Progression of Diabetic Nephropathy. Diabetes. 2019; 68: 1026–1039.
[19] Nunnari J, Suomalainen A. Mitochondria: in sickness and in health. Cell. 2012; 148: 1145–1159.
[20] Annesley SJ, Fisher PR. Mitochondria in Health and Disease. Cells. 2019; 8: 680.
[21] Fan Y, Yang Q, Yang Y, Gao Z, Ma Y, Zhang L, *et al*. Sirt6 Suppresses High Glucose-Induced Mitochondrial Dysfunction and Apoptosis in Podocytes through AMPK Activation. International Journal of Biological Sciences. 2019; 15: 701–713.
[22] Kong ZL, Che K, Hu JX, Chen Y, Wang YY, Wang X, *et al*. Orientin Protects Podocytes from High Glucose Induced Apoptosis through Mitophagy. Chemistry & Biodiversity. 2020; 17: e1900647.
[23] Cao Y, Chen Z, Hu J, Feng J, Zhu Z, Fan Y, *et al*. Mfn2 Regulates High Glucose-Induced MAMs Dysfunction and Apoptosis in Podocytes *via* PERK Pathway. Frontiers in Cell and Developmental Biology. 2021; 9: 769213.
[24] Su J, Gao C, Xie L, Fan Y, Shen Y, Huang Q, *et al*. Astragaloside II Ameliorated Podocyte Injury and Mitochondrial Dysfunction in Streptozotocin-Induced Diabetic Rats. Frontiers in Pharmacology. 2021; 12: 638422.
[25] Li Y, Ou S, Liu Q, Gan L, Zhang L, Wang Y, *et al*. Genistein improves mitochondrial function and inflammatory in rats with diabetic nephropathy via inhibiting MAPK/NF-κB pathway. Acta Cirurgica Brasileira. 2022; 37: e370601.
[26] Sinha K, Das J, Pal PB, Sil PC. Oxidative stress: the mitochondria-dependent and mitochondria-independent pathways of apoptosis. Archives of Toxicology. 2013; 87: 1157–1180.
[27] Rizwan H, Pal S, Sabnam S, Pal A. High glucose augments ROS generation regulates mitochondrial dysfunction and apoptosis via stress signalling cascades in keratinocytes. Life Sciences. 2020; 241: 117148.
[28] Qin X, Zhao Y, Gong J, Huang W, Su H, Yuan F, *et al*. Berberine Protects Glomerular Podocytes via Inhibiting Drp1-Mediated Mitochondrial Fission and Dysfunction. Theranostics. 2019; 9: 1698–1713.
[29] He JY, Hong Q, Chen BX, Cui SY, Liu R, Cai GY, *et al*. Ginsenoside Rb1 alleviates diabetic kidney podocyte injury by inhibiting aldose reductase activity. Acta Pharmacologica Sinica. 2022; 43: 342–353.
[30] Zhang T, Chi Y, Kang Y, Lu H, Niu H, Liu W, *et al*. Resveratrol ameliorates podocyte damage in diabetic mice via SIRT1/PGC-1α mediated attenuation of mitochondrial oxidative stress. Journal of Cellular Physiology. 2019; 234: 5033–5043.
[31] Yang X, Liu Q, Li Y, Tang Q, Wu T, Chen L, *et al*. The diabetes medication canagliflozin promotes mitochondrial remodelling of adipocyte via the AMPK-Sirt1-Pgc-1α signalling pathway. Adipocyte. 2020; 9: 484–494.
[32] Valero T. Mitochondrial biogenesis: pharmacological approaches. Current Pharmaceutical Design. 2014; 20: 5507–5509.
[33] Herzig S, Shaw RJ. AMPK: guardian of metabolism and mitochondrial homeostasis. Nature Reviews. Molecular Cell Biology. 2018; 19: 121–135.
[34] Carling D. AMPK signalling in health and disease. Current Opinion in Cell Biology. 2017; 45: 31–37.
[35] Wu M, Zhao A, Yan X, Gao H, Zhang C, Liu X, *et al*. Hepatic AMPK signaling dynamic activation in response to REDOX balance are sentinel biomarkers of exercise and antioxidant intervention to improve blood glucose control. eLife. 2022; 11: e79939.
[36] Chapnik N, Genzer Y, Ben-Shimon A, Niv MY, Froy O. AMPK-derived peptides reduce blood glucose levels but lead to fat retention in the liver of obese mice. The Journal of Endocrinology. 2014; 221: 89–99.
[37] Jia L, Li W, Li J, Li Y, Song H, Luan Y, *et al*. Lycium barbarum polysaccharide attenuates high-fat diet-induced hepatic steatosis by up-regulating SIRT1 expression and deacetylase activity. Scientific Reports. 2016; 6: 36209.
[38] Zheng Z, Bian Y, Zhang Y, Ren G, Li G. Metformin activates AMPK/SIRT1/NF-κB pathway and induces mitochondrial dysfunction to drive caspase3/GSDME-mediated cancer cell pyroptosis. Cell Cycle (Georgetown, Tex.). 2020; 19: 1089–1104.
[39] Chyau CC, Wang HF, Zhang WJ, Chen CC, Huang SH, Chang CC, *et al*. Antrodan Alleviates High-Fat and High-Fructose Diet-Induced Fatty Liver Disease in C57BL/6 Mice Model via AMPK/Sirt1/SREBP-1c/PPARγ Pathway. International Journal

Journal of
BIOLOGICAL REGULATORS
and Homeostatic Agents

of Molecular Sciences. 2020; 21: 360.

[40] Jalgaonkar MP, Parmar UM, Kulkarni YA, Oza MJ. SIRT1-FOXOs activity regulates diabetic complications. Pharmacological Research. 2022; 175: 106014.

[41] Sun HJ, Xiong SP, Cao X, Cao L, Zhu MY, Wu ZY, *et al*. Polysulfide-mediated sulfhydration of SIRT1 prevents diabetic nephropathy by suppressing phosphorylation and acetylation of p65 NF-κB and STAT3. Redox Biology. 2021; 38: 101813.

[42] Xue H, Li P, Luo Y, Wu C, Liu Y, Qin X, *et al*. Salidroside stimulates the Sirt1/PGC-1α axis and ameliorates diabetic nephropathy in mice. Phytomedicine: International Journal of Phytotherapy and Phytopharmacology. 2019; 54: 240–247.

[43] Ji J, Tao P, Wang Q, Li L, Xu Y. SIRT1: Mechanism and Protective Effect in Diabetic Nephropathy. Endocrine, Metabolic & Immune Disorders Drug Targets. 2021; 21: 835–842.

[44] Cantó C, Auwerx J. PGC-1alpha, SIRT1 and AMPK, an energy sensing network that controls energy expenditure. Current Opinion in Lipidology. 2009; 20: 98–105.

[45] Ye JX, Wang SS, Ge M, Wang DJ. Suppression of endothelial PGC-1α is associated with hypoxia-induced endothelial dysfunction and provides a new therapeutic target in pulmonary arterial hypertension. American Journal of Physiology. Lung Cellular and Molecular Physiology. 2016; 310: L1233–42.

[46] Hou S, Zhang T, Li Y, Guo F, Jin X. Glycyrrhizic Acid Prevents Diabetic Nephropathy by Activating AMPK/SIRT1/PGC-1α Signaling in db/db Mice. Journal of Diabetes Research. 2017; 2017: 2865912.

[47] Ruderman NB, Xu XJ, Nelson L, Cacicedo JM, Saha AK, Lan F, *et al*. AMPK and SIRT1: a long-standing partnership? American Journal of Physiology. Endocrinology and Metabolism. 2010; 298: E751–E760.

[48] Liao Z, Zhang J, Wang J, Yan T, Xu F, Wu B, *et al*. The anti-nephritic activity of a polysaccharide from okra (Abelmoschus esculentus (L.) Moench) via modulation of AMPK-Sirt1-PGC-1α signaling axis mediated anti-oxidative in type 2 diabetes model mice. International Journal of Biological Macromolecules. 2019; 140: 568–576.

[49] Eid AA, Ford BM, Block K, Kasinath BS, Gorin Y, Ghosh-Choudhury G, *et al*. AMP-activated protein kinase (AMPK) negatively regulates Nox4-dependent activation of p53 and epithelial cell apoptosis in diabetes. The Journal of Biological Chemistry. 2010; 285: 37503–37512.

[50] Sharma K, Ramachandrarao S, Qiu G, Usui HK, Zhu Y, Dunn SR, *et al*. Adiponectin regulates albuminuria and podocyte function in mice. The Journal of Clinical Investigation. 2008; 118: 1645–1656.

[51] Cai X, Bao L, Ren J, Li Y, Zhang Z. Grape seed procyanidin B2 protects podocytes from high glucose-induced mitochondrial dysfunction and apoptosis via the AMPK-SIRT1-PGC-1α axis *in vitro*. Food & Function. 2016; 7: 805–815.